Mechanism and Control of High-Intensity-Laser-Driven Proton Acceleration

T. Lin, K. Flippo, M. Rever, A. Maksimchuk, D. Umstadter

FOCUS Center, University of Michigan, Ann Arbor, MI 48109-2099, USA

Abstract. We discuss the optimization and control of laser-driven proton beams. Specifically, we report on the dependence of high-intensity laser accelerated proton beams on the material properties of various thin-film targets. Evidence of star-like filaments and beam hollowing (predicted from the electrothermal instability theory) is observed on Radiochromic Film (RCF) and CR-39 nuclear track detectors. The proton beam spatial profile is found to depend on initial target conductivity and target thickness. For resistive target materials, these structured profiles are explained by the inhibition of current, due to the lack of a return current. The conductors, however, can support large propagating currents due to the substantial cold return current which is composed of free charge carriers in the conduction band to neutralize the plasma from the interaction. The empirical plot shows relationship between the maximum proton energy and the target thickness also supports the return current and target normal sheath acceleration (TNSA) theory. We have also observed filamentary structures in the proton beam like those expected from the Weibel instability in the electron beam. Along with the ion acceleration, a clear electron beam is detected by the RCF along the tangent to the target, which is also the surface direction of target plate.

MOTIVATION

Proton acceleration from the ultrahigh-intensity-laser solid targets has been studied and attributable to electrostatic fields produced by hot electrons acting on protons from absorbed hydrocarbons[1]; however, in order to obtain higher energy proton source, it is required to understand what parameters are controlling the proton energy. First thing we are interested in is the relationship between maximum proton energy and ponderomotive potential of the incident laser pulse or the laser peak intensity. Former publication[2] showed a parametric study about maximum proton energy and ponderomotive potential by one laser facility. The least-square fitting to the data shows: up to 10^{18} Wcm^{-2} μm^2, the maximum ion energy scales as $(I\lambda^2)^{0.4}$ but when the oscillatory velocity of the fast electrons becomes relativistic (at about 10^{18} W/cm^2), the maximum ion energy scales as $(I\lambda^2)^{0.5}$. This result agrees with Fig. 1, which shows the fitting above 10^{18} Wcm^{-2} μm^2 from different laser facilities[3-18].

For many proton beam applications, we need a high-energy proton beam with small emittance. For example, for cancer therapy, radiologists want to take advantage of the small volume of laser proton accelerator for hadron radiation therapy; however, they need at least 250 MeV proton source to obtain good inhibition of growing of cancer cells. So far, the proton source from intensity of 10^{20} W/cm^2 laser pulse can provide a 30 MeV proton beam which is far below the minimum requirements for

CP737, *Advanced Accelerator Concepts: Eleventh Workshop,*
edited by Vitaly Yakimenko

hadron radiation therapy; therefore, besides increasing the laser energy and intensity, the optimization of the proton beam energy is very essential at this point.

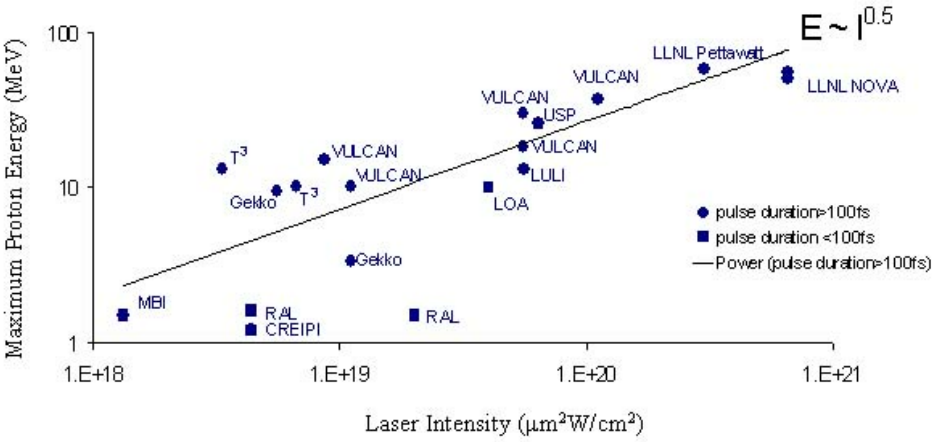

FIGURE 1. Relationship between maximum proton energy and laser intensity from different laser facilities label besides data points. This plot shows proton energy has a $I^{0.5}$ dependence on laser intensity.

PROTON FRONT & REAR-SIDE ACCELERATION

We have known the protons come from the hydrocarbons on the surface of the thin-film target; however, two different models of proton origin established. A. Maksimchuk *et al.*[19], Clark *et al.* [20] reported the protons are accelerated from the front side of the target surface; on the other hand, the target normal sheath acceleration (TNSA)[21] mechanism provide the explanation to the mechanism for the rear-side protons gaining energy from the front side hot electrons.

From our previous report[22], Fig. 2 showed a pronounced trend that maximum proton energy is related to the target thickness for both Mylar and aluminum targets. The dashed line in Fig. 2 is a fitting after the correction of linear energy transfer (LET) losses incurred in traversing thicker targets and the triangle and circles are the actual data. For thin targets and high-energy proton beam, this correction has almost no effect; therefore, we can see the dashed line did not change very much for energy above 5 MeV, or for thinner than 100 μm aluminum targets, or 25 μm Mylar targets. From this dashed line, we also can see there is a clear change from a peak to a plateau for aluminum targets thicker than 50 μm and 25 μm Mylar targets. This peak is a good evidence of TNSA model for rear-side proton acceleration, which means if the hot electrons from the front surface are energetic enough to be accelerated through the target plates to reach the rear-side surface, these electrons will also drag the protons from the rear-side of the target. These hot electrons are capable to accelerate protons to high energy level. If these electrons are able to flow back (recirculation current) to the front side of the target, they can be accelerated again through the electrostatic field

produced by the charge separation to a higher energy; therefore, the protons can be accelerated more to higher energy. On the other hand, when the electrons are not energetic enough to form a return current back to the front side of the target, only front-side protons will be accelerated when the first charge separation is established. This explains the plateau after a certain cutoff which is an inhibition of the return current.

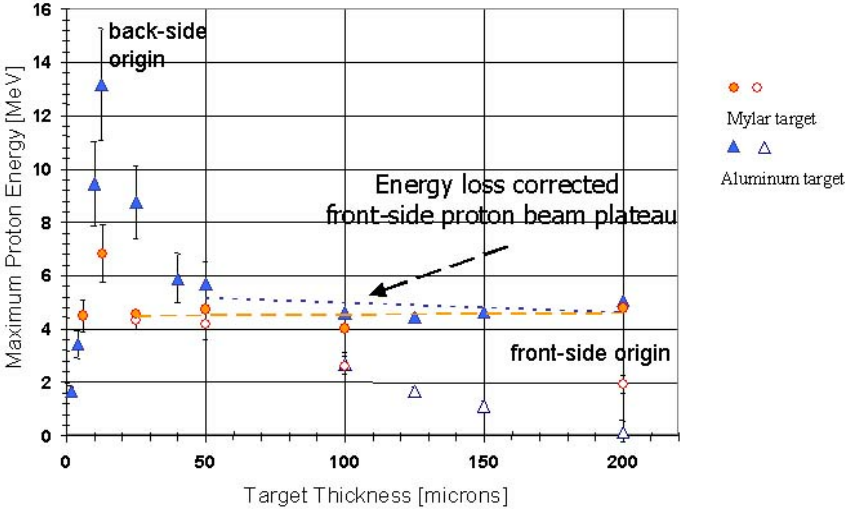

FIGURE 2. Plot of experimental results of maximum proton energy vs. target thickness for both Mylar target and aluminum target.

This provides a general idea that the lower energy tail of protons is from the front side acceleration; the higher energy cutoff is from the rear side acceleration. From Fig. 2, we can see the plateau happens at 5 MeV maximum proton energy, and the rear-side acceleration peak has about 13 MeV maximum proton energy. A recent simulation work[23] expects a similar result and has the same energy expectation for the front side proton- 5 MeV and rear side- 13 MeV for our laser condition. From Fig. 8 of Y. Sentoku's result [23], it showed the maximum proton energy from the rear side and the front side vs. the pulse length. At 400 fs pulse duration which is our laser condition, it showed there is a 13 MeV protons coming from rear side of the target plate, and 5 MeV protons coming form the front side. This is a good agreement to our proposed model, which is when the laser pulse hits the target, hot electrons are accelerated to penetrate through the target. Due to the tendency for plasma to be neutralized, some electrons will be bent back to the target to form a return current to go back to the front side of the target. When the returned electrons come back to the front side of the target within the laser pulse duration, these electrons are able to get accelerated again by the electrostatic fields built by the charge separation. Those electrons are capable to accelerate the protons to higher energy. Furthermore, if the electrons are fast enough to be recirculated in and out of the target, the electrons can gain more and more energy and the proton can be accelerated higher energy. And this also coincides with the target material difference that with higher conductivity

material targets, they can provide more free electrons to help recirculated current; therefore, higher conductivity materials can provide higher energy proton beam than resistive materials.

BEAM PROFILE DEPENDENCE ON TARGET MATERIAL AND THICKNESS

The spatial beam profile is a very essential point to control the proton beam- it provides the emittance and the laminarity of the proton beam. Target thickness and the target material are the main controls to affect the spatial beam profile.

During the time of charge separation establishing, the hot electrons will penetrate through the target. At this time, the different characteristics of the target material will start to affect the proton acceleration on both energy distribution and spatial profile. For conductive target, the conductivity is large, and from Ohm's law, $j = \sigma E$, it can support the propagation of electron beams which includes forward direction and the return currents. When the conductivity is low, the lack of the available free charge carriers will prevent the flow of a return current, and the propagating beam will lose energy quickly from Ohmic dissipation; therefore, the energy distribution will not be the same as conductors. Also, for the nonlinear and nonisotropic response from the resistive materials, a more structured proton beams are expected. Fig. 3 shows when the conductivity gets larger, the proton beam has smoother distribution, and each column image is the data for the same shot. The upper row are RCF images which can deposit lower energy proton and electrons. The lower row are CR-39 images which are covered by one layer of RCF shown above to corresponding images. The CR-39 can record the full range energy ions, and because of the RCF covered above, the CR-39 will record the higher energy part of proton beam. For both high and low energy parts of proton beam, it shows that the higher conductivity is, the proton beam profile has less structures. In terms of proton energy, from CR-39 images, the (h) in Fig. 3 has a saturation region at the center of the beam which is a good evidence that higher conductivity will al so provide higher energy of proton.

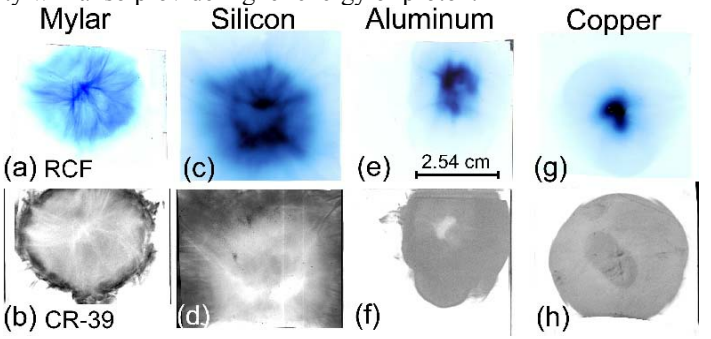

Figure 3. Each column is different target material. The conductivity of materials increases from left to right. Each column was taken at the same shot of laser. The upper row is scanned images from Radiochromic film (RCF) and the lower row is the scanned images from nuclear detector CR-39.

From Fig. 3, we also see the star pattern from lower conductive materials. Without or more difficult to have charge neutralization, the electric field begins to ionize the bulk dielectric leading to electrothermal and Weibal instabilities. A simulation done by L. Gremillet *et al.*[24] showed a similar image projected through 5 cm free space as our experimental data taken from RCF. The Fig. 5 in [24] showed a star-like feature of the electron beam. This simulated electron beam had a 10 μm FWHM Gaussian profile, a 405 fs rectangular pulse duration, an energy of 500 keV, and 10^{20} cm^{-3} which was similar to our T [3] laser condition. Our experimental data are shown in Fig. 4.

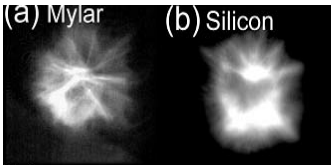

Figure 4. (a), (b) are our experimental proton beam images on RCF from Mylar and silicon targets.

For target thickness dependence, the aluminum target images are shown in Fig. 5.

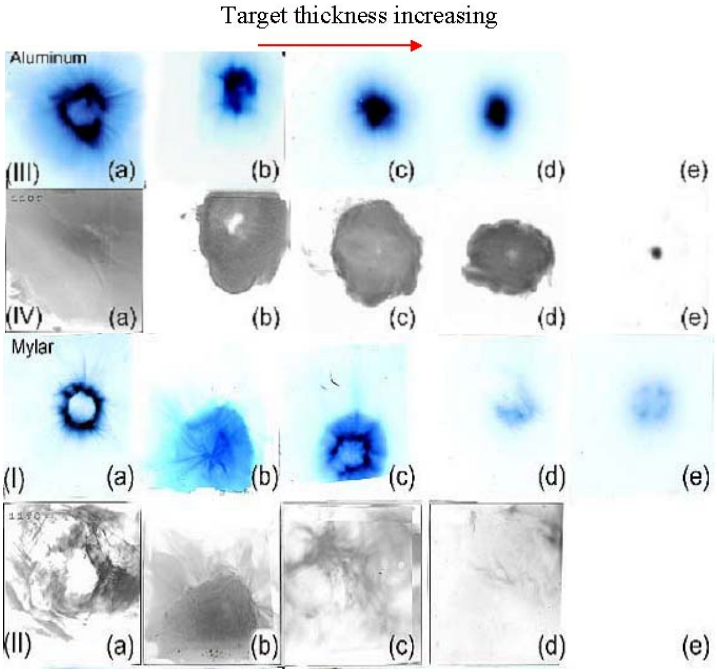

Figure 5. Mylar images on RCF (I) and CR-39 (II) varying in thickness:(a) 6 μm, (b) 13 μm , (c) 25 μm, (d) 50 μm, and (e) 100 μmAluminum images on RCF (III) and CR-39 (IV) varying in thickness: (a) 4 μm, (b) 12.5 μm, (c) 25 μm, (d) 50 μm, and (e) 75 μm[25]Compared to Fig. 2, we can notice that there is a proton energy peak at 12.5 μm and after the peak, the proton beam profile also shows a decrease of size which we discussed above about the energy loss inside the target.

ELECTRON ANGULAR DISTRIBUTION

Along with proton acceleration, the electrons are the drive for the whole acceleration process. Understanding the electron behavior is a good start to understand the good control of the proton beam profile and the energy distribution. Fig. 6 shows the experimental setup for the electron detection and the electron distribution layout from EDR2 x-ray film. A tendency for electrons to flow along the target plate is observed. It is a good indication that there is a surface current flowing along the tangential direction of the target plate. We put a magnet electron spectrometer to determine the electron energy, and it showed these electrons have energy up to 700 keV.

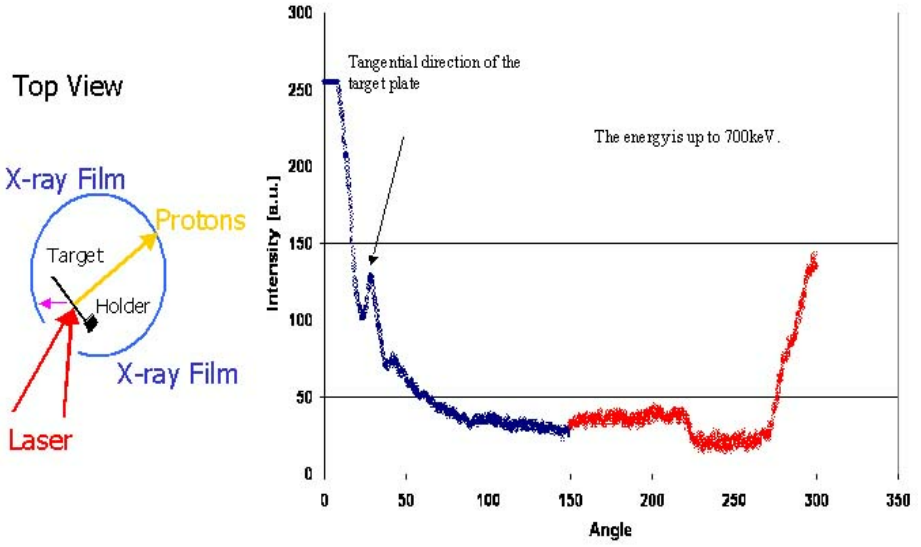

Figure 6. Electron detection from EDR2 x-ray films which were wrapped around the target plate. The intensity distribution layout shows that there is a tendency for electrons to flow at tangential direction of the target plate.

CONCLUSION

We discuss the optimization and control of laser-driven proton beams and there are two main parameters which affects the proton energy: (1) the thickness of the target-there is a optimum thickness for proton acceleration for different laser conditions; (2) the target material-higher conductive materials providing higher energy of protons. Each of them plays an essential role to control the proton beam quality. Along with the ion acceleration, a clear electron beam is detected by the RCF at the target tangential direction, which is also the surface direction of target plate.

ACKNOWLEGEMENT

We thank Y. Sentoku and L. Gremillet for providing helpful simulation works and discussion and acknowledged the support of the National Science Foundation.

REFERENCES

1. S. J. Gitomer *et al., Phys. Fluids* **29**, 2679 (1986).
2. E.L. Clark *et al., Phys. Rev. Letters*85, 1654 (2000).
3. T^3, Maksimchuk A PRL **84** 4108 (2000)
4. T^3, K. Nemoto APL **78** 596 (2001)
5. LULI ,Allen M POP **10** 3283 (2003)
6. GEKKO XII,M Habara et. al PoP **10** 3712 (2003)
7. Gekko MII Y. Murakami PoP **8** 4138 (2001)
8. VULCAN M. Zepf PoP **8** 2323 (2001)
9. VULCAN M. Zepf PoP **8** 2323 (2001)
10. VULCAN,Borghesi M APL **82** 1529 (2003)
11. VULCAN,Clark EL PRL **84** 670 (2000)
12. VULCAN, Krushelnick K PoP **7** 2055 (2000)
13. LLNL RA Snavely PRL **85** 2945 (2000)
14. Nucl. Instr.&Methd. In Phys. Res. A **464** (2001)
15. Nucl. Instr.&Methd. In Phys. Res. A **455**(2000)
16. MBI kHz, Thoss JOSAB **20** 224 (2003)
17. Nd:Glass, J Badziak PRL **87** 215001 (2001)
18. Nd:Glass Badziak J JAP **91** 5504 (2002)
19. A. Maksimchuk *et al., Phys. Rev. Lett*. **84**, 4108 (2000)
20. E.L. Clark *et al. Phys. Rev. Lett***. 84,** 670 (2000)
21. S.C. Wilks *et al*. *Phys. Plasmas* **8,** 542 (2001)
22. K. Flippo *et al.* Proceedings of Tenth Advanced accelerator Conference, C.E. Clayton and P. Muggli, eds, 2002, CP647, pp 255-261
23. Y. Sentoku *et al. ,Phys. Plasmas,* **10,** 2009 (2003)
24. L. Gremillet *et al., phys. Plasma* **9**, 941 (2002)
25. K. Flippo dissertation for degree of Doctor of Philosophy (Nuclear Engineering and Radiological Sciences) in The University of Michigan 2004